Dissociation dynamics of transient anion formed via electron attachment to sulfur dioxide

K. Gope, V. S. Prabhudesai, N. J. Mason, and E. Krishnakumar

Citation: The Journal of Chemical Physics **147**, 054304 (2017);
View online: https://doi.org/10.1063/1.4994899
View Table of Contents: http://aip.scitation.org/toc/jcp/147/5
Published by the American Institute of Physics

Dissociation dynamics of transient anion formed via electron attachment to sulfur dioxide

K. Gope,[1] V. S. Prabhudesai,[1] N. J. Mason,[2] and E. Krishnakumar[1,a)]
[1]*Tata Institute of Fundamental Research, Homi Bhabha Road, Colaba, 400005 Mumbai, India*
[2]*School of Physical Sciences, The Open University, Walton Hall, Milton Keynes MK7 6AA, United Kingdom*

(Received 1 March 2017; accepted 8 July 2017; published online 3 August 2017)

We report the molecular dynamics of dissociative electron attachment to sulfur dioxide (SO_2) by measuring the momentum distribution of fragment anions using the velocity slice imaging technique in the electron energy range of 2–10 eV. The S^- channel results from symmetric dissociation which exhibits competition between the stretch mode and bending mode of vibration in the excited parent anion. The asymmetric dissociation of parent anions leads to the production of O^- and SO^- channels where the corresponding neutral fragments are formed in their ground as well as excited electronic states. We also identify that internal excitation of SO^- is responsible for its low yield at higher electron energies. *Published by AIP Publishing.* [http://dx.doi.org/10.1063/1.4994899]

I. INTRODUCTION

Sulfur dioxide (SO_2) is of atmospheric relevance as it is one of the main pollutants[1] in the troposphere[2] and the main precursor of acid rain. A substantial amount of SO_2 is produced from volcanic eruptions, which leads to clustering with positive and negative ions in the troposphere[2] and the creation of sulfate cloud condensation nuclei. This constitutes a significant control on climate via their strong influence on cloud droplet size, indeed the cooling is similar to the effect of warming due to CO_2,[3] influencing the overall temperature and the climate of the Earth.[4] Thus it is essential to understand the microscopic level chemical reactions which influence the climate involving SO_2 in our atmosphere. Due to the abundance of free electrons in the Earth's atmosphere, their interaction with SO_2 is of fundamental interest in atmospheric chemistry. Furthermore the presence of SO_2 in the atmosphere of the planet Jupiter[5] and its satellite Io and as a major component of the atmosphere of the planet Venus apart from being identified in interstellar clouds[6] makes the e-SO_2 interaction important in astronomical studies.

SO_2 is also an important precursor in several industrial processes. Sulfur ions in pulsed ion lasers are created using SO_2.[7] SO_2 also appears as a trace impurity in laser gases where the lasing process is initiated by electron beam injection mechanisms. Interaction of low-energy electrons with SO_2 is very important for modeling low-energy plasmas. It is used in electrical-discharges[8] to remove pollutants from industrial fumes. SO_2 is also important for the understanding of physics and chemistry of combustion.

Due to above relevance, dissociative electron attachment (DEA) to SO_2 has been studied extensively. DEA to SO_2 results in O^-, S^-, and SO^- channels. The very first measurement of DEA to SO_2 was performed by Rallis and Goodings[9] in 1971. They reported two peaks at 5.0 eV and 7.4 eV in the O^- channel with onset at 4.2 eV and 6.3 eV, respectively. Based on the kinetic energy (KE) analysis of O^- ions, they inferred that both the peaks have the same dissociation limit involving SO in its ground state. Harland *et al.*[10] reported considerably lower kinetic energy in the O^- channel and attributed this to vibrational excitation of SO. The two peaks observed in the O^- channels were explained due to the formation of SO in $X^3\Sigma^-$ and $a^1\Delta$ states and those in the SO^- channel due to O in the ^3P and ^1D states, respectively. Abouaf and Fiquet-Fayard[11] measured the ion yield curves of all the anions from SO_2 formed with near-zero KE and observed the fine structure in the ion yield curve related to the formation of the SO diatomic fragment in excited vibrational states. In the O^- channel, they obtained two series of structures in the ion yield curve around the first peak which they assigned due to vibrational excitation of SO ($X^3\Sigma^-$) and SO ($a^1\Delta$). In the S^- channel also, they observed two structures which they assigned as being due to the formation of O_2 ($X^3\Sigma_g^-$) up to v = 4 and $O_2(a^1\Delta_g)$ up to v = 3. Nandi and Krishnakumar[12] measured the kinetic energies of O^- ions by analyzing the peak width in time of flight spectrum and concluded that both the peaks in the ion yield curve are due to dissociation to the same limit although they did not rule out the possibility of the SO ($a^1\Delta$) limit as suggested by Abouaf and Fiquet-Fayard.[11] Nandi and Krishnakumar[12] also concluded that the potential energy surface of the SO_2^- state at 4.6 eV in the Frank-Condon region has a minimum, whereas for the second peak, it is repulsive.

Due to computational difficulties in calculating the potential energy surfaces of the anion of polyatomic molecules, very little is known about these excited anion states although they play a significant role in atmospheric chemistry as well as plasma environment. Studies of the dynamics of the dissociative electron attachment can provide valuable information about the potential energy surfaces of the underlying excited anion states. Here we report details of the DEA dynamics of the sulfur dioxide molecule.

Note: This article was intended as part of the Special Topic "Developments and Applications of Velocity Mapped Imaging Techniques" in Issue 1 of Volume 147 of J. Chem. Phys.

a)Electronic mail: ekkumar@tifr.res.in

II. EXPERIMENTAL TECHNIQUES

The experimental setup used for these measurements has been described earlier.[13–15] In brief, a magnetically collimated and pulsed (200 ns wide) electron beam is made to cross at right angles with an effusive molecular beam produced by a capillary along the axis of the Velocity Slice Imaging (VSI) spectrometer. The spectrometer consists of a single element electrostatic lens and a drift tube. In order to avoid stray magnetic field, the entire spectrometer along with the other elements of the housing assembly is made of titanium. The VSI spectrometer is followed by a 2D position sensitive detector (PSD) that consists of a set of three 75 mm diameter micro-channel plates mounted in a Z-stack configuration, and a phosphor screen. The ions formed in the interaction volume are extracted by a pulsed electric field. This pulsed field is put on 100 ns after the electron beam pulse. The central slice of the Newton sphere of the ions formed is recorded by keeping the detector in the detection mode for only 100 ns by applying a 2 kV pulse to the detector coinciding with the arrival time of the anions. The images formed on the phosphor screen are recorded by a CCD camera. From these momentum images, the kinetic energy and angular distributions are determined. The uncertainty in the electron beam energy used in the experiment is ±0.35 eV which translates as an equivalent uncertainty in the measured kinetic energy release (KER) in the process.

III. RESULTS AND DISCUSSION

SO_2 belongs to the C_{2v} point group in its equilibrium geometry, and its ground state is of A_1 symmetry with a bond angle of 119.3°[16] and a bond length of 0.143 nm. It has a positive electron affinity of 1.097 eV. All possible DEA channels along with their threshold are presented in Table I.

The thermodynamic thresholds are calculated from the bond dissociation energy (BDE) of SO–O = 5.69 eV[17] and BDE (O–O) = 5.11 eV[18] and the electron affinity (EA) of O = 1.46 eV, EA (SO) = 1.15 eV, and EA (S) = 2.07 eV.[19,20] The zero point energy of SO ($a^1\Delta$) and SO ($b^1\Sigma^+$) with respect to that of SO ($X^3\Sigma^-$) is 0.79 eV and 1.5 eV, respectively,[21] and the zero point energy of $O_2(a^1\Delta_g)$ and $O_2(b^1\Sigma_g^+)$ with respect to that of $O_2(X^3\Sigma_g^-)$ is 0.98 eV and 1.68 eV, respectively. The energy of $O(^1D)$ and $O(^1S)$ with respect to $O(^3P)$ is 1.1 eV and 4.2 eV, respectively.

TABLE I. DEA channels in SO_2 along with their energy thresholds.

No.	Dissociation channels	Threshold (eV)
1	$SO_2 + e^- \rightarrow O^- + SO(X^3\Sigma^-)$	4.3
2	$SO_2 + e^- \rightarrow O^- + SO(a^1\Delta)$	5.1
3	$SO_2 + e^- \rightarrow O^- + SO(b^1\Sigma^+)$	5.6
4	$SO_2 + e^- \rightarrow O^- + S(^3P) + O(^3P)$	9.7
5	$SO_2 + e^- \rightarrow SO^- + O(^3P)$	4.6
6	$SO_2 + e^- \rightarrow SO^- + O(^1D)$	5.7
7	$SO_2 + e^- \rightarrow SO^- + O(^1S)$	8.8
8	$SO_2 + e^- \rightarrow S^- + O_2(X^3\Sigma_g^-)$	3.9
9	$SO_2 + e^- \rightarrow S^- + O_2(a^1\Delta_g)$	4.8
10	$SO_2 + e^- \rightarrow S^- + O_2(b^1\Sigma_g^+)$	5.5
11	$SO_2 + e^- \rightarrow S^- + O(^3P) + O(^3P)$	9
12	$SO_2 + e^- \rightarrow O_2^- + S(^3P)$	5.5

The mass spectrum of DEA to SO_2 exhibits 3 peaks: mass 16(O^-), 32 (S^- or O_2^-), and 48 (SO^-). O^- is the most dominant ion peaking at 4.6 eV and 7.2 eV. SO^- peaks at 4.8 eV and 7.3, whereas S^- or O_2^- peaks at 4.2 eV, 7.4 eV, and 9 eV. The dissociation of SO_2^- may proceed via two-body or three-body fragmentation. However for electron energies up to 9 eV, we rule out the three-body dissociation channel based on threshold energy (Table I). Since the threshold energy for O_2^- formation is 5.5 eV, the 4.2 eV peak in the ion yield of mass 32 can safely be attributed to S^-. Throughout the second peak in the excitation function (7.4 eV), we observe a low kinetic energy in a mass 32-channel. This implies substantial vibrational excitation of the molecular fragment. As the electron affinity of O_2 is 0.44 eV, O_2^- with substantial vibrational excitation will not survive against auto-detachment, and hence we attribute this peak to S^- ions. Below we discuss the S^-, O^-, and SO^- channels separately.

A. O^- channel

As mentioned above, the O^- channel is the most dominant DEA channel observed with peaks in the ion yield curve at 4.6 eV and 7.2 eV. We have recorded momentum images from 4.9 eV to 8.9 eV. Since the threshold for O^- formation through three-body fragmentation is 9.7 eV, the possible channels for the formation of O^- in this energy range correspond to the formation of SO in the ground or lowest two electronic excited states (see Table I). Throughout this energy range, the O^- momentum images obtained show an isotropic "blob" which increases in size with electron energy. From the momentum images, we have determined the kinetic energy (KE) of the fragment. In the case of two-body breakup, the kinetic energy release (KER) is determined based on the conservation of linear momentum. It is given by

$$KER = \frac{(M_1 + M_2)}{M_2} \times KE_1 = \frac{(M_1 + M_2)}{M_1} \times KE_2, \quad (1)$$

where KE_i is the kinetic energy of fragment of mass M_i. KER distributions obtained from the momentum images are plotted in Fig. 1.

O^- formation in a two-body breakup dynamics necessarily requires the departure of the terminal O atom. We call this

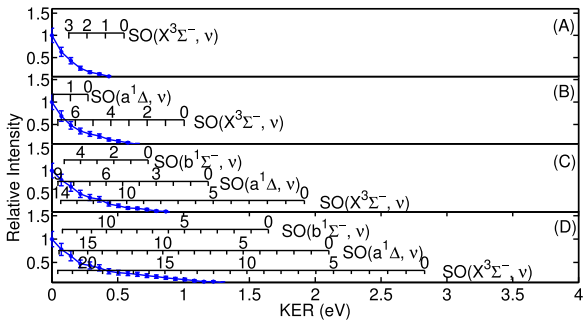

FIG. 1. Kinetic energy release (KER) obtained from the momentum images of O^- at electron energies (a) 4.9 eV, (b) 5.4 eV, (c) 6.4 eV, and (d) 7.4 eV. The expected KER of O^- with SO formed in various vibronic states is also shown.

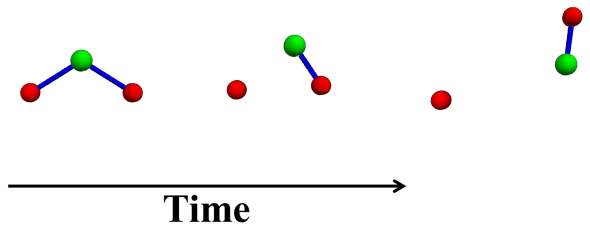

FIG. 2. Schematic diagram of time evolution of the asymmetric dissociation process. Here red spheres are for oxygen atoms and green sphere is for sulfur atoms.

the asymmetric dissociation as this will be a manifestation of the asymmetric stretch mode of vibration of the parent transient anion. With the bend geometry in the neutral ground state, such a breakup will necessarily provide a kick to the molecular fragment along the line of the breaking bond (Fig. 2). This will result in the rotational motion of the molecular fragment. The extent of the rotation of the SO fragment depends on the bond angle of the parent molecule, the momentum of the O^- fragment, and the mass ratio of the two fragments. Under the simple impact approximation, assuming dissociation takes place at the equilibrium geometry of the molecule and ignoring the role of bending mode of vibration, the rotational kinetic energy of the SO fragment is given by

$$E_{Rot} = \frac{E_{Excess}}{\left(\frac{f}{\cos^2(\beta-90)} + 1\right)}, \quad (2)$$

where β is the bond angle of the dissociating OSO^- ion, $f = \frac{2M_O M_S + M_S^2}{M_O^2}$, where M_S is the mass of S and M_O is the mass of O. E_{Excess} is the excess energy available in the system which is given by

$$E_{Excess} = E_e - E_{Threshold}, \quad (3)$$

where $E_{Threshold}$ is the threshold energy for a given channel and E_e is the electron energy. For SO_2, this rotational energy would be $\frac{1}{11.6}$ of E_{Excess}. More details are given in the supplementary material.

Subtracting this rotational energy from the excess energy available to the system at a given electron energy, we obtain the net energy available for the vibrational and electronic degrees of freedom of the system as well as the translational motion of the fragments. In Fig. 1, we show the measured KER in the O^- channel along with the expected KER for various vibrational excitations of the SO fragment after subtracting its rotational energy. Here the vibrational levels for the SO molecule are determined based on the anharmonic oscillator model. The plot clearly shows that for both the peaks in the ion yield curve, the SO fragment is produced with very little kinetic energy indicating higher vibrational excitation of the SO fragment in the ground electronic state. Indeed the energy may be sufficient for the formation of electronically excited SO fragments ($a^1\Delta$ and $b^1\Sigma^+$), the excess energy showing up as the vibrational excitation. The vibrational excitation of the SO fragment is an indication of the role of symmetric and antisymmetric modes of vibrations of the parent transient anion. The high vibrational excitation of the SO fragment indicates the dominance of the asymmetric stretch mode, whereas lower vibrational excitation may be due to comparable strengths of both symmetric and asymmetric stretch modes.

B. SO^- channel

The SO^- ion yield peaks at 4.8 eV and 7.3 eV, and we have obtained momentum images across these two peaks. In this energy range, SO^- can be formed with an O atom in either a ^3P or ^1D state (Table I). In the 4.5 eV to 5 eV region, the momentum image of an SO^- anion appears as a thermal and isotropic blob as seen in Fig. 3(a). In this energy range, SO^- is formed with O (^3P). Since the image is an isotropic blob, we cannot determine the symmetry of the transient anion state involved in this channel. As the electron energy is increased above 5.5 eV, a new feature emerges, in the form of an outer

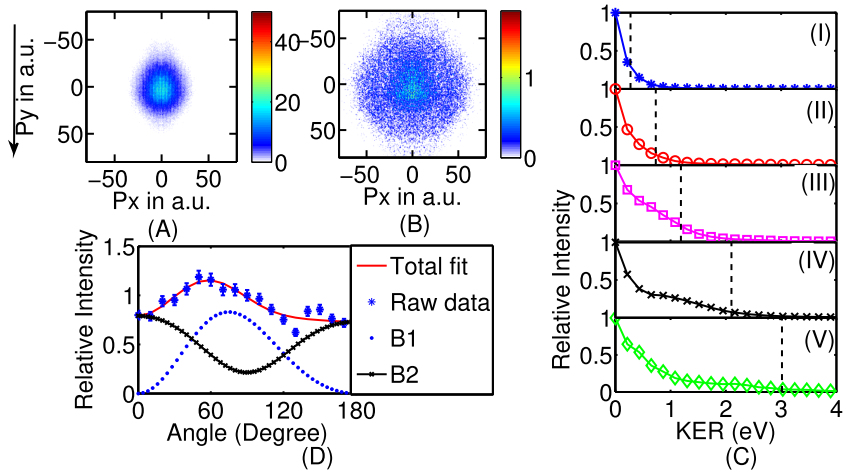

FIG. 3. The momentum images of SO^- at (a) 4.9 eV and (b) 6.9 eV. The vertical arrow indicates the direction of the electron beam. (c) The KER determined from the momentum images at electron energies of (I) 4.9 eV, (II) 5.4 eV, (III) 5.9 eV, (IV) 6.9 eV, and (V) 7.9 eV. The vertical line in each subplot in (c) indicates the maximum KER (after subtracting the rotational energy of SO^- under a simple impulse model) expected for the channel with the lowest threshold. The tail of the KER beyond this point is due to the finite energy resolution of the experiment with maximum contribution coming from the electron energy spread. (d) The angular distribution obtained for the SO^- ions with respect to the electron beam for the kinetic energy more than 0.35 eV at 6.9 eV electron energy. The plot also shows the fit to the angular distribution obtained using contributions from B_1 and B_2 states of the parent anion.

ring along with the inner blob, as shown in Fig. 3(b). From the momentum distributions at various electron energies, we have obtained the KER distributions which are plotted in Fig. 3(c). From this figure, we can see that for electron energies beyond 5.5 eV, the contribution from the outer ring appears as an additional hump. The two structures in the KER spectrum indicate the opening up of an extra channel along with the lower energy channel. From the KE analysis, we identify the inner blob to be due to the $SO_2 + e^- \rightarrow SO^- + O\ (^1D)$ channel, whereas the outer ring is due to the $SO_2 + e^- \rightarrow SO^- + O\ (^3P)$ channel. Since the inner structure is an isotropic blob, we are unable to specify any symmetry of the transient anion involved in this process. However, for the outer ring, we can determine the symmetry of the transient anion state contributing to this channel.

We obtain the symmetry of the transient anion state by employing the formalism presented by O'Malley and Taylor[22] for the diatomic case and modified by Azria *et al.*[23] for the polyatomic species. The angular distribution of the fragment ions is given by the expression

$$I(\theta) \propto \frac{1}{2\pi}\int_0^{2\pi} |\sum_{lm\epsilon} i^l \exp(i\delta_l) a^{\epsilon}_{lm} X^{\epsilon^*}_{lm}(\theta,\phi)|^2 d\phi, \qquad (4)$$

where $X^{\epsilon^*}_{lm}(\theta,\phi)$ is the basis function for the irreducible representation of the group of the molecule, a^{ϵ}_{lm} is their amplitude, and δ_l is their phase. Here, the angle (θ,ϕ) determines the orientation of the dissociating bond with respect to the incoming electron beam. These functions are in the dissociation frame of the molecule and are expressed as a linear combination of the spherical harmonics with appropriate frame transformations from the lab frame to the molecular frame.

The measured and fitted angular distributions at 6.9 eV are shown in Fig. 3(d). As can be seen from the figure, the angular distribution is not symmetric about 90° with respect to the electron beam. As the molecule does not possess the inversion symmetry about the dissociation axis, all odd and even partial waves would contribute to the electron capture process. The coherent contribution of these partial waves may manifest in the forward backward asymmetry in the angular distribution as observed in this case. We have used a linear combination of spherical harmonics corresponding to B_1 and B_2 irreducible representation of the C_{2v} point group with bond angle 119.3° for the fit. It can be seen that both the states have comparable intensity. Thus, we may conclude that the second peak has contributions from transient anions of both B_1 and B_2 symmetries.

Since SO^- can only form via asymmetric dissociation, it will be rotationally excited just like in the case of O^- formation. We have plotted in Fig. 3 the KER obtained at a given electron energy along with the expected maximum KER after subtracting the rotational energy of the SO^- fragment under the simple impulse model. As can be seen from Fig. 3, the KER accounts for the substantial part of the excess energy of the system across the first peak of the ion yield curve. For the second peak in the ion yield curve, the observed KER is found to be much lower than the total excess energy available in the system. This implies that the SO^- fragment is formed with vibrational excitation.

C. S^- channel

In our electron energy range of interest, the S^- yield peaks at 4.2 eV and 7.2 eV. Across the first peak, we consistently find the momentum image to be a simple structureless blob. KER distributions at 4.9 eV and 5.9 eV are shown in Fig. 4. As can be seen from these KER distributions, the excess energy in the system appears as the vibrational excitation of the molecular O_2 fragments. Based on the energy thresholds (see Table I), the ion signal at 4.9 eV corresponds predominantly to the formation of O_2 in $X^3\Sigma_g^-$. Previous kinetic energy measurements[11] indicated that at 5.9 eV, S^- may also be formed with O_2 in the $a^1\Delta_g$ or $b^1\Sigma_g^+$ state. This would imply that there may be more than one resonance contributing to this peak. In either case, the excess energy partitioning prefers vibrational excitation of molecular fragments.

The momentum images of S^- across the second peak also appear as blobs but with a larger diameter as compared to those at the first peak. The corresponding KER distributions are shown in Fig. 4. Similar to the first peak, the molecular fragment [O_2 ($X^3\Sigma_g^-$ or $a^1\Delta_g$)] is formed with vibrational excitation across this peak. As the electron energy increases, the excess energy appears as higher vibrational excitation as against the KER.

The S^- formation from SO_2^- by two-body dissociation requires terminal oxygen atoms to come together. This is made possible by combination of the symmetric stretch and bending modes of vibrations of parent anions as shown in Fig. 5. If during this bending and symmetric stretching of the OSO^- molecule the terminal O atoms come close enough to form a bond, it results in the formation of O_2. Consequently the parent anion dissociates into $S^- + O_2$, and this is symmetric dissociation. The vibrational excitation of O_2 formed is determined by the extent of bending mode excitation as against the symmetric stretch mode. The fragments thus formed acquire low kinetic energy as a substantial part of the excess energy goes into the vibrational excitation of O_2. We observe that the vibrational excitation of O_2 increases with electron energy as the corresponding KER does not show an equivalent increase. This indicates that with increasing electron energy, the energy transfer into the bending mode vibration increases. As this is observed across both the peaks in the S^- ion yield curve, we conclude that the competition between the bending and stretching modes of vibration is relevant in the dissociation dynamics

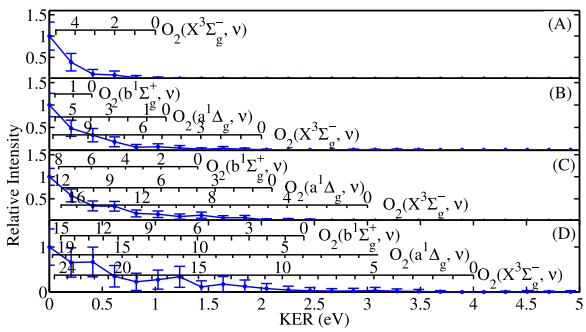

FIG. 4. Kinetic energy release (KER) determined from the momentum images of S^- obtained at electron energies of (a) 4.9 eV, (b) 5.9 eV, (c) 6.9 eV, and (d) 7.9 eV. The expected KER of S^- with O_2 formed in various vibronic states is also shown.

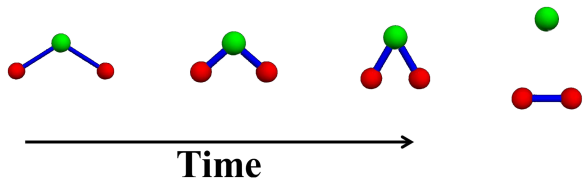

FIG. 5. Schematic diagram of time evolution of the symmetric dissociation process. Here red spheres are for oxygen atoms and green sphere is for sulfur atoms.

of all the anion states accessed by the electron capture leading to S^- formation. This may imply that the potential energy surfaces of anion states contributing to both peaks in the S^- ion yield curve follow similar landscapes.

IV. CROSS SECTION AND DYNAMICS

Both O^- and SO^- anions are produced via asymmetric dissociation with two peaks in each of these ion yields. These peak positions are at almost identical electron energies (4.6 eV and 7.2 eV for O^- and 4.8 and 7.3 eV for SO^-). The O^- cross sections[24] at both the peaks are comparable as seen in Fig. 6(a). However for the case of SO^-, the cross section of the second peak is much lower than the first peak.

The KE distribution of SO^- ions obtained from the momentum images taken at 7.9 eV electron energy is shown in Fig. 6(b). The contributions from the $SO^- + O(^1D)$ channel and the $SO^- + O(^3P)$ channel are clearly separated in the KE spectrum and have been fitted using Gaussian profiles. The ratio of the area under both the curves is the branching ratio of these channels leading to SO^-. The vertical line marked as Y represents the expected maximum KE of the SO^- ions with $O(^3P)$ as the other fragment when all the excess energy is showing up as the translational energy of the fragments. As the SO^- ground state is only 1.1 eV below the SO neutral state, energy in excess of this as the internal energy of SO^- will cause the auto-detachment of the extra electron. The corresponding limit on the KE of SO^- ions has been shown by the vertical line marked as X in Fig. 6(b). The uncertainties in the positions of these lines are about ±0.1 eV. The difference between X and Y lines in Fig. 6(b) indicates the maximum allowed energy in the SO^- fragment as internal energy (1.1 eV). This implies that if any SO^- is produced with KE below the X line via the $SO^- + O(^3P)$ channel it would be too short lived to be detected. Based on this, we may conclude that the second peak of SO^- in the ion yield curve is produced via both channels but a large fraction of the low threshold channel may not be detected due to loss via auto-detachment of the anion fragment. This may explain the relatively low cross section observed in the SO^- channel at the second peak.

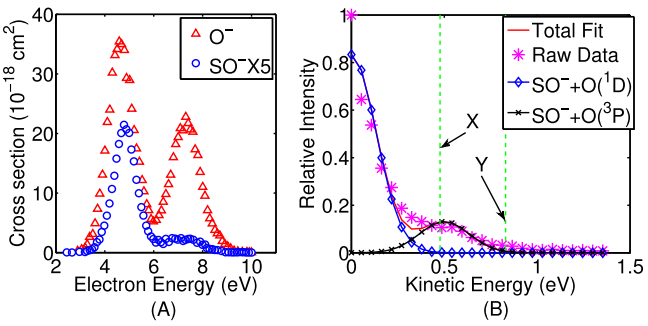

FIG. 6. (a) Absolute cross section of various fragment anion formation via DEA to SO_2 (Krishnakumar *et al.*[24]) and (b) KE distribution of SO^- ions obtained at 7.9 eV electron energy. The distribution is fitted using two Gaussians for the contributions from the two possible channels appearing with different kinetic energy values. The vertical lines indicate the maximum KE of SO^- ions expected for the channel with $O(^3P)$ (Y) and correspondingly minimum KE of SO^- ions with excess energy appearing as its vibrational excitation without the autodetachment of the electron (X).

It can also be noted that the overall cross section measured for the S^- channel is about 2 orders of magnitude lower than the O^- channel and about an order of magnitude lower than the SO^- channel. The S^- formation is a consequence of the symmetric dissociation of the transient anion which also involves significant bending motion, whereas the O^- and SO^- fragments are formed due to asymmetric dissociation of the transient anion where the stretch modes of vibrations dominate. As the cross sections are peaking in the same electron energy range, we conclude that the lifetime of the transient anion states leading to DEA signal has a substantially lower lifetime against auto-detachment for the topology of the potential energy surface corresponding to the bending mode of vibration as compared to the stretch modes.

V. CONCLUSION

To conclude, we have determined the dissociation dynamics of the excited anion states that result in various fragment channels in the DEA to SO_2. The production of S^- proceeds via symmetric dissociation of the parent anion resulting in vibrational excitation of the O_2 fragment. This channel shows the signature of competition between the bending and stretching modes of vibrations of the parent anion state. The O^- and SO^- channels result from the asymmetric dissociation. Here the corresponding neutral fragments are formed in their electronic ground as well as excited states with considerable vibrational excitation of the diatomic fragment. The kinetic energy distribution of SO^- shows that the relatively low cross section for SO^- formation at the 7 eV resonance is due to its large vibrational excitation and subsequent autoionization. The kinetic energies and angular distributions measured for various fragment channels reflect the nature of potential energy surfaces of these transient anion states which are extremely difficult to determine by any *ab initio* calculations.

SUPPLEMENTARY MATERIAL

See supplementary material for the derivation of the rotational energy transfer to the diatomic fragment during dissociation.

ACKNOWLEDGMENTS

One of us (N.J.M.) acknowledges the support of FP7 European project ITN Lassie Grant Agreement No. 238258 during the development of this work and the H2020 Twinning project "Achievement of Excellence in Electron Processes for Future

Technologies"(ELEvaTE) Grant Agreement No. 692335 for collaborative discussions.

[1]I. M. Cadez, V. M. Pejcev, and M. V. Kurepa, J. Phys. D: Appl. Phys. **16**, 305 (1983).
[2]R. B. Chatfield and P. J. Crutzen, J. Geophys. Res.: Atmos. **89**, 7111, doi:10.1029/jd089id05p07111 (1984).
[3]A. Zecca, J. C. Nogueira, G. P. Karwasz, and R. S. Brusa, J. Phys. B: At., Mol. Opt. Phys. **28**, 477 (1995).
[4]T. M. L. Wigley, Nature **339**, 365 (1989).
[5]K. B. Jefferts, A. A. Penzias, R. W. Wilson, and P. M. Solomon, Astrophys. J. **168**, L111 (1971).
[6]A. F. Cheng, Astrophys. J. **242**, 812 (1980).
[7]J. Marling, IEEE J. Quantum Electron. **14**, 4 (1978).
[8]W. C. Wang and L. C. Lee, J. Chem. Phys. **84**, 2675 (1986).
[9]D. A. Rallis and J. M. Goodings, Can. J. Chem. **49**, 1571 (1971).
[10]P. W. Harland, J. L. Franklin, and D. E. Carter, J. Chem. Phys. **58**, 1430 (1973).
[11]R. Abouaf and F. Fiquet-Fayard, J. Phys. B: At. Mol. Phys. **9**, L323 (1976).
[12]D. Nandi and E. Krishnakumar, Int. J. Mass Spectrom. **289**, 39 (2010).
[13]E. Szymańska, V. S. Prabhudesai, N. J. Mason, and E. Krishnakumar, Phys. Chem. Chem. Phys. **15**, 998 (2013).
[14]K. Gope, V. S. Prabhudesai, N. J. Mason, and E. Krishnakumar, J. Phys. B: At., Mol. Opt. Phys. **49**, 015201 (2015).
[15]K. Gope, V. Tadsare, V. S. Prabhudesai, N. J. Mason, and E. Krishnakumar, Eur. Phys. J. D **70**, 134 (2016).
[16]S. Barsotti, M.-W. Ruf, and H. Hotop, Phys. Rev. Lett. **89**, 083201 (2002).
[17]M. Ivanco, J. Hager, W. Sharfin, and S. C. Wallace, J. Chem. Phys. **78**, 6531 (1983).
[18]G. Herzberg, *Molecular Spectra and Molecular Structure* (Van Nostrand, Princeton, 1957).
[19]A. A. ChristodouIides, D. L. McCorkle, and L. G. Christophorou, *Electron-Molecule Interactions and Their Applications* (Academic, New York, 1984).
[20]P. M. Dehmer and W. A. Chupka, J. Chem. Phys. **62**, 4525 (1975).
[21]R. Colin, Can. J. Phys. **46**, 1539 (1968).
[22]T. F. O'Malley and H. S. Taylor, Phys. Rev. **176**, 207 (1968).
[23]R. Azria, Y. L. Coat, G. Lefevre, and D. Simon, J. Phys. B: At. Mol. Phys. **12**, 679 (1979).
[24]E. Krishnakumar, S. V. K. Kumar, S. A. Rangwala, and S. K. Mitra, Phys. Rev. A **56**, 1945 (1997).